

Simultaneously All-Optical Inverted and Noninverted Wavelength Conversion Employing Ultra-Small Silicon-on-Insulator Waveguide

Jianwei Wu · Fengguang Luo ·
Cristiano de Mello Gallep · Shyh-Lin Tsao

Received: 20 September 2007 / Accepted: 26 November 2007 /

Published online: 12 December 2007

© Springer Science + Business Media, LLC 2007

Abstract We propose single-to-dual all-optical wavelength conversion based on stimulated Raman effect on silicon waveguides. Simulation results of non-return-to-zero (NRZ) pseudorandom bit sequence (2^7 –1 code) at 10, 50, and 200-Gbit/s rates of conversion in an ultra-small silicon-on-insulator waveguide are presented. The main goal in the proposed scheme is that the converted signal can be obtained simultaneously inverted, at the 1550 nm channel (down-conversion) and non-inverted, at the 1846 nm channel (up-conversion), for original signal fixed at 1686 nm.

Keywords Integrated optics · Silicon-on-insulator · Wavelength conversion · Simulation

1 Introduction

In recent times, some studies have demonstrated silicon as an ideal platform for optoelectronic integrated devices due to some practical features, including its stimulated Raman scattering (SRS), 10^4 times higher than that of silica glass fibers because of the single crystal structure [1–5]. However, nonlinear losses due to the indirect band gap structure - including two photon absorption (TPA) and free carrier absorption (FCA),

J. Wu (✉) · F. Luo

Institute of Optoelectronics Science and Engineering & Wuhan National Laboratory for Optoelectronics, Huazhong University of Science and Technology, Wuhan 430074, People's Republic of China
e-mail: jwwu@smail.hust.edu.cn

C. de Mello Gallep

Telecommunication Technology Division/CESET, State University of Campinas, Limeira, SP, Brazil

S.-L. Tsao

Optical Fiber System Laboratory, Institute of Electro-optical Science and Technology,
National Taiwan Normal University, Taipei, Taiwan, Republic of China

induced by TPA - are limiting factors for optical communication applications. To overcome the nonlinear loss induced by carrier, some approaches such as the reverse biased p-i-n junction, pulsed pumping and scaling down of waveguide dimension among others were reported, with success in decreasing the carrier lifetime [6–8].

All-optical communication networks will need, in a not so distant future, to be very dynamic in traffic management, relocating data transfer over the available physical and spectral pathways, enabling as deep as possible a better utilization of the installed network and with minimum hardware, i.e., high costs. The cheapest and most matured semiconductor technology is, for sure, that of silicon and related procedures. Silicon photonics are being used to implement lasers, detectors, ring resonators and very good waveguides. Among the many interesting features of Si-based photonics, wavelength conversion is one of the nonlinear applications of great interest. Up to now many wavelength conversion devices have been investigated, some based on cross-gain modulation (XGM), cross-phase modulation (XPM) and four-wave mixing (FWM) in non-linear devices such as semiconductor optical amplifiers (SOA) and special optical fibers [9–12].

In this way, Si-photonics are the most suitable approach for integrated high-speed all-optical signal conversion because the signal distortion induced by dispersion can be ignored for ultrashort picosecond pulse in only several millimeters or centimeters long silicon waveguides [13]. Many previous reports focus on single-to-single channel conversion, operating with inverted or non-inverted modulation, but some recent researches present results of single-to-dual and simultaneous inverted and non-inverted conversion [14–16]. However, the designed devices are not so easily used in high integration schemes. In this paper a novel project is proposed and simulated the single-to-dual and simultaneously inverted and non-inverted wavelength conversion at 10, 50, and 200-Gb/s rates by using SRS in highly integrated ultra-small SOI optical waveguide, which has the advantages of lower Raman threshold and smaller nonlinear loss.

2 Model and theory

To perform the wavelength conversion, the SOI rib waveguide adopted is shown in Fig. 1 where the rib structure is beneficial for reducing the signal loss and supporting the single mode operation comparing with the conventional strip waveguide [17, 18], which has the width w , rib height H , and slab height h , the center wavelength of primary signal wave λ_s ,

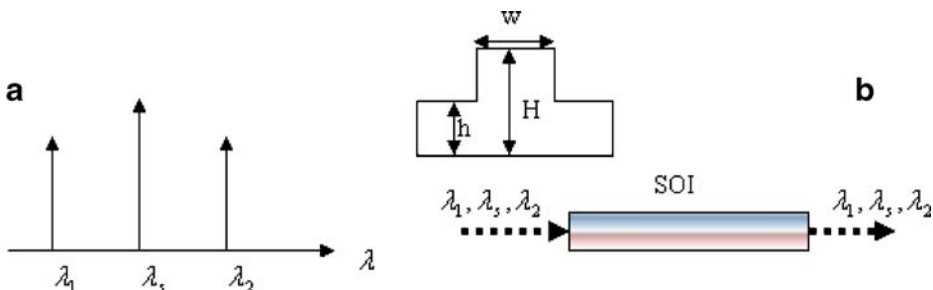


Fig. 1 Schematic diagram of invert and non-invert wavelength conversion based on SOI.

λ_1 , and λ_2 are the probe continuous-waves (CW). To obtain higher SRS gain and high quality wavelength conversion, the three wavelengths will be selected accurately due to Raman gain peak frequency shift of 15.6 THz in silicon waveguide. So the λ_s should lie near the Raman gain spectrum peak of λ_1 , and λ_2 should lie near the Raman gain spectrum peak of λ_s .

The present model is similar to the standard model used to describe Raman fiber amplifier [19], but will include additional terms describing the effects of TPA, and FCA. So we generalize the differential equations describing the longitudinal variation of the primary signal pulse and two CW probe waves inside the SOI waveguide by taking into account SRS and including linear absorption loss, TPA and FCA. Therefore, when neglecting the interaction between λ_1 and λ_2 due to enough spectral distance, the optical intensity change along the waveguide may be described as:

$$\frac{dI_1}{dz} = \left(-\alpha - g_s \frac{\lambda_s}{\lambda_1} I_s - \beta I_1 - 2\beta I_s - \sigma n \right) I_1 \quad (1)$$

$$\frac{dI_s}{dz} = [-\alpha + g_s(I_1 - I_2) - 2\beta I_s - 2\beta(I_1 + I_2) - \sigma n] I_s \quad (2)$$

$$\frac{dI_2}{dz} = \left(-\alpha + g_s \frac{\lambda_s}{\lambda_2} I_s - \beta I_2 - 2\beta I_s - \sigma n \right) I_2 \quad (3)$$

where z is transmission distance, α is linear absorption loss, g_s is Raman gain coefficient for λ_s in silicon waveguide, λ is wavelength, β is TPA coefficient, σ is the free carrier absorption cross section, n is the free carrier density. The time dependence of the free carrier density in the silicon waveguide can be written as [20]:

$$\frac{dn}{dt} = -\frac{n}{\tau_{eff}} + \frac{\beta}{2h_p c} (\lambda_1 I_1^2 + \lambda_s I_s^2 + \lambda_2 I_2^2) \quad (4)$$

where h_p is Planck constant, c is the light velocity in vacuum, τ_{eff} is the effective carrier life, which is denoted by [21]

$$\tau_{eff}^{-1} = \frac{S}{H} + \frac{w + 2(H - h)}{wH} S' + 2 \frac{h}{H} \sqrt{\frac{D}{w^2} \left(\frac{S + S'}{h} \right)} \quad (5)$$

where the first term refers to the interface recombination lifetime, the second term refers to the surface recombination at the sidewalls, and last term refers to transit time out of the modal area. S and S' are the effective surface recombination velocity, D is diffusion coefficient.

To present quality of conversion signal, the eye-opening width, i.e., relative eye amplitude ratio, is calculated, in logarithmic scale, defined by

$$A_{eye} = 10 \log \frac{bit_1^{\min} - bit_0^{\max}}{bit_0^{\max}} \quad (6)$$

where A_{eye} has the unit of dB, bit_1^{\min} and bit_0^{\max} denote respectively the lower “1”-bit level and the higher “0”-bit level of conversion signals.

Table 1 Simulation Parameters.

Parameter	Definition	Value
α	Waveguide linear loss coefficient	0.22 dB/cm
g_s	Raman gain at 1686 nm	59×10^{-9} cm/W
L	Waveguide length	4.2 mm
β	Two-photon absorption coefficient	0.44 cm/GW
σ	Free carrier absorption cross section	1.45×10^{-17} cm ²
W	Rib-waveguide width	445 nm
H	Rib height	500 nm
h	Slab height	220 nm
S, S'	Effective surface recombination velocity	80 m/s
D	Diffusion coefficient	16 cm ² /s
C	Light velocity in vacuum	2.99792458×10^8 m/s
h_p	Planck constant	6.63×10^{-34} J·s
λ_s	Primary signal wavelength	1686 nm
λ_1	Probe wavelength	1550 nm
λ_2	Probe wavelength	1848 nm

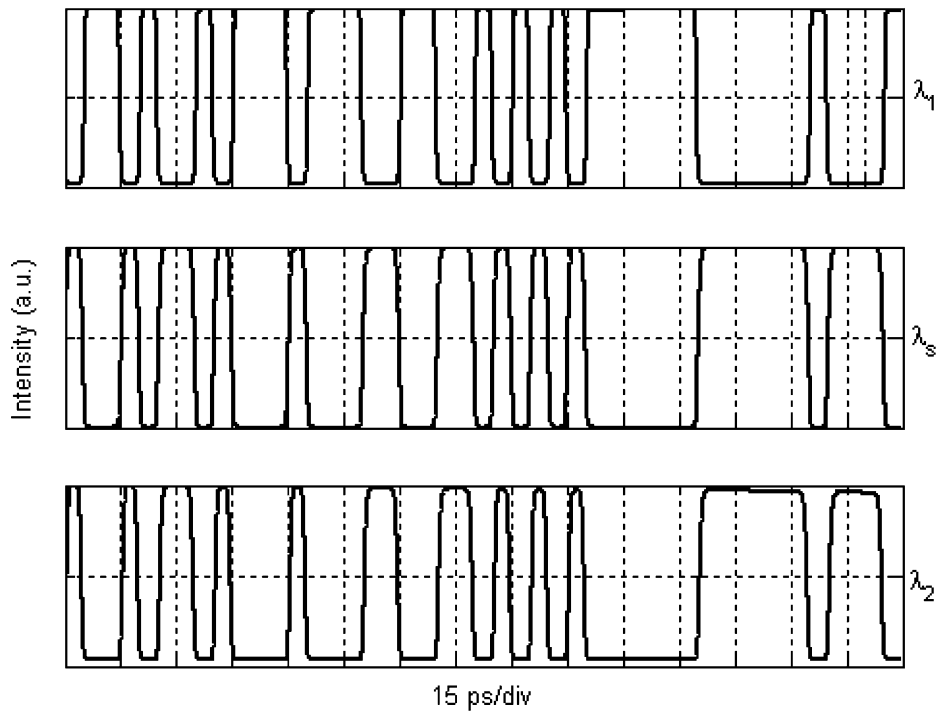
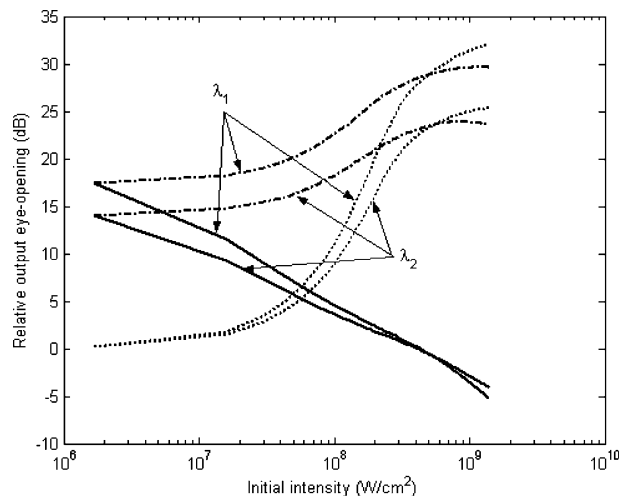
**Fig. 2** Waveforms of invert and non-invert wavelength conversion based on SOI with initial intensity 1.67×10^8 W / cm², 1.67×10^6 W/cm², and 1.67×10^6 W/cm² for optical field λ_s , λ_1 and λ_2 , respectively.

Fig. 3 Variation curves of eye-opening for inverted and non-inverted signal versus the initial intensity of each channel. The solid lines as a function of initial intensity at λ_2 for fixed $1.67 \times 10^8 \text{ W/cm}^2$ at λ_s and $1.67 \times 10^6 \text{ W/cm}^2$ at λ_1 . The dotted lines as a function of initial intensity at λ_1 for fixed $1.67 \times 10^8 \text{ W/cm}^2$ at λ_s and $1.67 \times 10^6 \text{ W/cm}^2$ at λ_2 . The dashed lines as a function of initial primary signal intensity for fixed two probe wave intensities of $1.67 \times 10^6 \text{ W/cm}^2$.

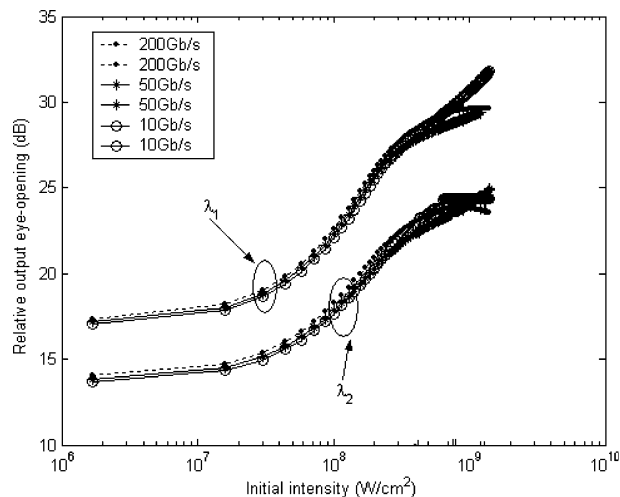


3 Simulation results

Equations (1–6) can be solved numerically by 4th-order Runge-Kutta (RK) algorithm [22], in simulation, the all parameters are listed in Table 1.

When three optical fields are simultaneously co-propagating in waveguide, the single-to-dual and inverted and noninverted wavelength conversion can be achieved by SRS effect. Figure 2 shows the time domain waveforms of initial primary signal and output conversion signal pulses at 200-Gb/s. From the figure, it is shown that the inverted signal at 1550 nm and noninverted signal at 1848 nm are simultaneously achieved after going through the waveguide. These imply that the energy will transfer from λ_1 to λ_2 , and from λ_s to λ_2 due to SRS process when co-propagating in SOI waveguide. Furthermore, the transfer efficiency is proportional to the overlapped optical energy between adjoining two optical fields, which will enhance as increasing the overlapped energy.

Fig. 4 Variation curves of eye-opening for inverted and non-inverted signal versus the initial intensity of λ_1 at different bit rates.



To describe the code pattern quality of conversion signals, eye-opening of system is a very important parameter [22], so the variation curves of eye amplitude ratio (eye-opening) versus the original signal intensity and intensities of probe waves are shown in Fig. 3 for inverted and non-inverted signal pulses, respectively. From the Fig. 3, it is shown that the eye amplitude ratio will sub-linearly increase with increasing the intensity at λ_2 or λ_1 for a fixed intensity at λ_2 , and monotonically decrease with increasing the intensity at λ_2 for fixed other optical field intensities. These can be explained that the SRS will be enhanced as increase in the optical intensities at λ_s and λ_1 , and energy which will be transferred from λ_1 to λ_s , and from λ_s to λ_2 , respectively, as a result that the eye-opening width is also improved. But when increasing the optical intensity at λ_2 , the optical intensity at λ_s will rapidly decrease due to SRS between λ_s and λ_2 . So, more energy of the primary signal will be transferred to λ_2 so as to decrease the eye-opening width. In addition, some other features should be adverted from the figure. One case is that when increasing further the initial intensity at λ_1 or λ_s , eye amplitude ratio will begin to decay due to the enhanced nonlinear loss and gain saturation. Another case is that the eye amplitude ratio will be negative value with increasing further the incident intensity at λ_2 which implies that the conversion signal is strongly distorted under the condition.

In fact, intensity of the incident primary signal is low during wavelength conversion. So, In order to achieve more wide eye-opening, we can suitably increase the intensity at λ_1 . At the same time, the conversion efficiency of inverted signal is also improved. The correspond variation curves of eye-opening for conversion signals are shown in Fig. 4 at 10, 50, and 200-Gb/s rates, respectively. In this figure, we can see that the width of eye-opening will be increased with increasing the optical intensity at λ_1 where the eye-opening of conversion signal is insensitive to the different rates for low launching intensity owing to the small nonlinear loss, but becomes dependent on the bit rates for high input intensity because of the combined effects of nonlinear loss and gain saturation.

4 Conclusion

We have reported simulations of single-to-dual and simultaneously inverted and non-inverted wavelength conversion signal, obtained by using stimulated Raman scattering process in ultra-small silicon-on-insulator optical waveguide at 10, 50, and 200-Gb/s rates with 2^{7-1} pseudorandom code. Moreover, the conversion signals have well pulse waveforms and wide eye-opening ratio. The model of ultra-small silicon-on-insulator optical waveguide may be selected for high-speed wavelength conversion in highly integrated optoelectronic device.

Acknowledgement This work was supported by the Chinese Natural Science Foundation under grant. No. 60677023.

References

1. H. K. Tsang, C. S. Wong, and T. K. Liang, Optical dispersion, two-photon absorption and self-phase modulation in silicon waveguides at 1.5 μm wavelength. *Appl. Phys. Lett.* **80**, 416–418 (2002).
2. G. W. Rieger, K. S. Virk, and J. F. Young, Nonlinear propagation of ultrafast 1.5 μm pulses in high-index-contrast silicon-on-insulator waveguides. *Appl. Phys. Lett.* **84**, 900–902 (2004).

3. H. Rong, R. Jones, A. Liu, O. Cohen, D. Hak, A. Fang, and M. Paniccia, A continuous-wave Raman silicon laser. *Nature* **433**, 725–728 (2005).
4. L. Yin, Q. Lin, and G. P. Agrawal, Dispersion tailoring and soliton propagation in silicon waveguides. *Opt. Lett.* **31**, 1295–1297 (2006).
5. E. Culurciello, Three-dimensional phototransistors in 3D silicon-on-insulator technology. *Electron. Lett.* **43**, 418–420 (2007).
6. H. Rong, A. Liu, R. Jones, O. Cohen, D. Hak, R. Nicolaescu, A. Fang, and M. Paniccia, An all-silicon Raman laser. *Nature* **433**, 292–294 (2005).
7. A. Liu, H. Rong, M. Paniccia, O. Cohen, and D. Hak, Net optical gain in a low loss silicon-on-insulator waveguide by stimulated Raman scattering. *Opt. Express* **12**, 4261–4268 (2004).
8. R. L. Espinola, J.I. Dadap, R.M. Osgood, S. J. Mcnab, and Y. A. Vlasov, Raman amplification in ultrasmall silicon-on-insulator wire waveguides. *Opt. Express* **12**, 3713–3718 (2004).
9. C. M. Gallep, A.L.R. Cavalcanti, N. Ribeiro, and E. Conforti, Nonhomogeneous current injection for the enhancement of semiconductor optical amplifier-based wavelength converters. *Microw. Opt. Technol. Lett.* **48**, 1141–1144 (2006).
10. J. Dong, S. Fu, X. Zhang, P. Shum, L. Zhang, and D. Huang, Analytical solution for SOA-based all-optical wavelength conversion using transient cross-phase modulation. *IEEE Photonics. Technol. Lett.* **18**, 2554–2556 (2006).
11. H. Simos, I. Stamatakis, and D. Syvridis, Relative intensity noise performance of wavelength converters based on four-wave mixing in semiconductor optical amplifiers. *IEEE J. Quantum Electron.* **43**, 370–377 (2007).
12. P. A. Andersen, T. Tokle, Y. Geng, C. Peucheret, and P. Jeppesen, Wavelength conversion of a 40-Gb/s RZ-DPSK signal using four-wave mixing in dispersion-flattened highly nonlinear photonic crystal fiber. *IEEE Photonics. Technol. Lett.* **17**, 1908–1910 (2005).
13. Q. Xu, V. R. Almeida, and M. Lipson, Demonstration of high Raman gain in a submicrometer-size silicon-on-insulator waveguide. *Opt. Lett.* **30**, 35–37 (2005).
14. J. Wang, and J. Sun, All-optical single-to-dual channel wavelength conversion based on sum-frequency generation and difference-frequency generation. *Microw. Opt. Technol. Lett.* **48**, 2057–2060 (2006).
15. J. Wang, and J. Sun, Simultaneous observation of inverted and noninverted wavelength conversion of picosecond pulses in LiNbO₃ waveguides. *Microw. Opt. Technol. Lett.* **49**, 295–298 (2007).
16. Z. Chen, J. Wu, K. Xu, and J. Lin, Simultaneously all-optical inverted and noninverted wavelength conversion employing SOA-based sagnac interferometer. *Microw. Opt. Technol. Lett.* **49**, 547–551 (2007).
17. A. G. Rickman, G. T. Reed, and F. Namavar, Silicon-on-insulator optical rib waveguide loss and mode characteristics. *J. Lightwave Technol.* **12**, 1771–1776 (1994).
18. J. Lousteau, D. Furniss, A. B. Seddon, T. M. Benson, A. Vukovic, and P. Sewell, The single-mode condition for silicon-on-insulator optical rib waveguides with large cross section. *J. Lightwave Technol.* **22**, 1923–1929 (2004).
19. J. A. Yeung, and A. Yariv, Theory of CW Raman oscillation in optical fiber. *J. Lightwave Technol.* **69**, 803–807 (1979).
20. A. Liu, H. Rong, R. Jones, O. Cohen, D. Hak, and M. Paniccia, Optical amplification and lasing by stimulated Raman scattering in silicon waveguides. *J. Lightwave Technol.* **24**, 1440–1455 (2006).
21. D. Dimitropoulos, R. Jhaveri, R. Claps, J. C. S. Woo, and B. Jalali, Lifetime of photogenerated carriers in silicon-on-insulator rib waveguides. *Appl. Phys. Lett.* **86**(1–3), 07115(2005).
22. C. M. Gallep, A. C. Bordonalli, and E. Conforti, Simulation and measurements of current-injected gain control in semiconductor optical amplifiers. *Microw. Opt. Technol. Lett.* **41**, 477–481 (2004).